AN ABSTRACT OF THE THESIS OF

Inyong Kim for the degree of Master of Science in Electrical and Computer Engineering presented on December 6, 2023.

Title: Modeling of Wave Energy Converter via Instantaneous Frequency

Abstract approved: ______________________________________

Ted Brekken Yue Cao

A multidisciplinary perspective is necessitated for the analysis of wave energy conversion systems, spanning hydrodynamics, mechanics, electric power, and control systems. The complexity inherent in these scientific domains poses challenges for unified analysis. This paper addresses these challenges by connecting various domains through the application of circuit theory, characterizing the multiphysics system as an equivalent circuit. The methodology is exemplified using the two-body Reference Model 3 (RM3) Wave Energy Converter (WEC). Initially, equations of motion for each body are formulated, encompassing all six degrees of freedom, resulting in a model with 12 degrees of freedom. Subsequently, selective Eigenmode approximation analysis is employed to reduce the model to two modes, visualized as an equivalent circuit. Simulation results facilitate the comparison between the equivalent circuit model and the original full-order model.

Furthermore, to enhance the accuracy of WEC modeling and overcome limitations in analogies between mechanical and electrical components, this paper introduces Instantaneous Frequency Modeling (IFM). Improved modeling accuracy and the facilitation of testing various control methods are achieved through IFM. Leveraging the principle of electrical resonance, specifically impedance matching, enables the optimization of wave energy harvesting by controlling the force on the power take-off unit. Simulation results from the instantaneous model are presented, and performance under diverse control techniques is investigated.

Modeling of Wave Energy Converter via Instantaneous Frequency

by

Inyong Kim

A THESIS

submitted to

Oregon State University

in partial fulfillment of
the requirements for the
degree of

Master of Science

Presented December 6, 2023
Commencement June 2024

Master of Science thesis of Inyong Kim presented on December 6, 2023.

APPROVED:

Co-Major Professor, representing Electrical and Computer Engineering

Co-Major Professor, representing Electrical and Computer Engineering

Head of the School of Electrical Engineering and Computer Science

Dean of the Graduate School

ACKNOWLEDGEMENTS

This work was supported by the DOE Water Power Technologies Office under Grant #EE0009446.

CONTRIBUTION OF AUTHORS

Nasim Adami is the co-author of the first manuscript.

TABLE OF CONTENTS

TABLE OF CONTENTS (Continued)

LIST OF FIGURES

LIST OF FIGURES (Continued)

LIST OF TABLES

Chapter 1: General Introduction

Ocean waves hold substantial energy potential, benefiting from the fact that about 70 percent of the Earth's surface is covered by the ocean. Unlike solar and wind energy, which encounter constraints due to irregular energy harvesting—solar energy is limited to the daytime, and wind energy exhibits notable fluctuations—the shortcomings of these renewable sources present challenges in fully replacing traditional methods of energy generation. The demand for energy requires a level of consistency and stability that is not always met by solar and wind power. Notably, the ocean wave exhibits a characteristic of consistency. This consistency could aid in meeting energy needs on time. However, harvesting energy from ocean waves poses several challenges, including issues with energy transmission, maintenance, and the complexity of multi-physics interactions. Specifically, the installation of underwater cables incurs substantial costs, access to devices is hindered by their offshore locations, and optimization necessitates consideration of mechanical, hydrodynamical, electromechanical, and electrical principles.

Addressing these challenges relies on the effective modeling of Wave Energy Converters (WEC), where a robust model can simultaneously tackle cost, maintenance, and optimization issues. A proposed approach involves a unified physics model represented as an equivalent circuit for WEC to maximize energy harvest [2]. This modeling strategy capitalizes on the mathematical identity highlighting similarities between mechanical systems and electrical circuits. Furthermore, the application of the maximum energy transfer principle in electrical theory is integrated into the equivalent circuit to optimize the performance of the WEC.

Nevertheless, the application of equivalent circuit modeling is constrained primarily to regular wave scenarios, given the assumption that electrical components possess passive constant values. While the analysis of regular wave cases is straightforward, it tends to be less practical since real sea conditions seldom conform to regular patterns. To address this limitation, the concept of instantaneous frequency is introduced. This concept not only preserves the simplicity of regular wave analysis but also enhances the accuracy of equivalent circuit modeling, even in irregular sea conditions such as JONSWAP and Pierson-Moskowitz spectrum waves.

Furthermore, the novel modeling technique introduces the potential for real-time optimization of the Power-Take-Off unit, contrasting with the traditional assumption of constant wave frequency. This innovative approach offers opportunities for improved performance in the dynamic and unpredictable conditions of real sea environments.

Chapter 2: Manuscript 1

2.1 Introduction

Design of *wave energy conversion* (WEC) systems is particularly challenging due to the various disciplines involved. The fluid dynamics from waves entail complex physics and associated high-dimensional models. Mechanical systems require careful design to properly absorb wave energy and moving parts are coupled to electromechanical machines that convert energy from mechanical into electrical form. Electrical waveforms and electromagnetically-induced torque are shaped by power electronics drives and their onboard control systems. The performance and efficiency of the overall system strongly depend on how these aforementioned subsystems interact with one another. Given that each physical discipline has its own set of techniques and jargon, it is difficult to perceive the overall WEC under a unified perspective that clearly elucidates how the coupled systems operate. To bypass this issue, this paper is focused on translating each subsystem into an equivalent circuit such that the overall system can be visualized as a circuit. We place a strong focus on the derivation of a reduced order model for the wave-to-mechanical coupling and conclude with simulation results on a two-body Reference Model 3 (RM3) WEC system with drive controls.

The dynamical interactions between waves and mechanical structures are particularly complex and are generally studied through a combination of numerical simulations and/or analytical formulations. Numerical approaches that capture three-dimensional physics typically rely on formulations tailored toward partial differential equations associated with fluid mechanics. These include boundary element and finite element approaches [5]. Although these software simulations provide high-resolution results, they are computationally burdensome and may obscure intuition that might be gleaned from a more compact model [15]. On the other hand, analytical models may provide deeper insight but generally require a higher level of mathematical sophistication and are not as accurate as high-order numerical simulations [4].

Mathematically-driven methods for the control and design of WECs, such as those pursued in this paper, are generally predicated on the use of simplified models [12]. Towards that end, reduced-order models for hydro-mechanical physics have received significant attention. Such approaches include proper orthogonal decomposition [13], principal component analysis [6], and Eigenvalue or modal decomposition [9]. Despite considerable reductions in model complexity, contemporary software packages (e.g., WEC-Sim simulator [14]) must still numerically solve differential equations across six degrees of freedom for each moving body and a simple mathematical model is still out of reach.

In this paper, we address the aforementioned shortcomings through the use of Eigenvalue-based modal decomposition with the aim of reducing the number of degrees of freedom. We focus on the RM3 [14] point absorber system and show that the simplified hydro-mechanical model lends itself to a basic circuit representation that emphasizes the most important mechanics in the system. Furthermore, the novel instantaneous-frequency model is developed and implemented to further enhance the accuracy of the condition at the particular field considered.

2.2 Equivalent Circuit Representation

2.2.1 Governing Equation of RM3

Determining the motion of bodies for a WEC is highly interdisciplinary, integrating concepts from hydrodynamics, mechanics, electronics, and electromagnetism. Ignoring mooring and drag forces, the governing equation for the RM3 is

$$\mathbf{m}\ddot{\mathbf{x}}(t) = \mathbf{F}_{\text{ex}}(t) + \mathbf{F}_{\text{rad}}(t) + \mathbf{F}_{\text{rs}}(t) + \mathbf{F}_{\text{pto}}(t) \tag{2.1}$$

in which $\mathbf{F}_{\text{ex}}$ is the excitation force of the wave exerting on the bodies, $\mathbf{F}_{\text{rad}}$ is the radiation force, $\mathbf{F}_{\text{rs}}$ is the restoring force about the equilibrium point of the floating body, and $\mathbf{F}_{\text{pto}}$ is the electromagnetic force induced by the linear generator. Solving hydrodynamics using Finite Element Analysis for the Navier-Stokes equation is computationally expensive, particularly over the long durations common to WEC testing. To mitigate this issue, a structural analysis approach via the boundary element method for input-output is commonly implemented [14]. In the frequency domain, the radiation force can be modeled as $\mathbf{F}_{\text{rad}}(\omega) = -\mathbf{M}_{\text{add}}(\omega)\ddot{\mathbf{x}}(\omega) - \mathbf{B}_{\text{rad}}(\omega)\dot{\mathbf{x}}(\omega)$, in which $\mathbf{M}_{add}$ represents the added mass coefficient matrix, $\mathbf{B}_{rad}$ is the radiation damping coefficient matrix and the

w is the frequency of the incoming wave. These coefficients can be determined by experiment or numerical analysis. In this project, we use the coefficients calculated from wave analysis in Massachusetts Institute of Technology [10]. The hydrostatic restoring force is typically proportional to the displacement of the body relative to the sea surface, such that: $\mathbf{F}_{\mathrm{rs}}(t) = -\mathbf{K}\mathbf{x}(t)$, in which K is the hydrostatic coefficient matrix. The total mass matrix can be presented as $\mathbf{m} + \mathbf{M}_{\mathrm{add}}(\omega) = \mathbf{M}(\omega)$ by superposition, in which m is the dry mass of the RM3. The PTO force can be modeled in any form, depending on the corresponding controller. This paper considers pure damping control, where the force is proportional to the relative speed between two bodies in the heave direction. Through the superposition of damping terms, the total damping coefficient matrix is given as $\mathbf{B}_{\mathrm{rad}}(\omega) + \mathbf{B}_{\mathrm{pto}} = \mathbf{B}(\omega)$.

2.2.2 Equivalent Circuit Representation

It can be observed that an analogy can be made between forces and motion, and voltage and current. For example, note the same proportional relationships of $F = m\frac{dv}{dt}$ and the current-voltage relationship of a capacitor $I = C\frac{dV}{dt}$. Under this analogy, we can think of force as analogous to current, mass to capacitance, and velocity to voltage. Further analogous relationships can be drawn as shown in Table 3.1.

The control law of the generator, and the force it provides as a function of velocity or position, for example, can also be represented as a circuit subsystem [2].

The governing equation of the RM3 is translated from the hydrodynamics terms

Table 2.1: Mechanical to Electrical Analogy

Mechanical	$\leftrightarrow$	**Electrical**
Force [N]	$\leftrightarrow$	Current [A]
Velocity [m/s]	$\leftrightarrow$	Voltage [Volts]
Mass [kg]	$\leftrightarrow$	Capacitance [F]
Damping [N/(m/s)]	$\leftrightarrow$	1/Resistance [1/Ohms]
Stiffness [N/m]	$\leftrightarrow$	1/Inductance [1/Henries]

to the equivalent circuit representation, as shown in the following equation:

$$\mathbf{I}(t) = \mathbf{C}\dot{\mathbf{V}}(t) + \frac{1}{\mathbf{R}}\mathbf{V}(t) + \frac{1}{\mathbf{L}}\int \mathbf{V}(t)\,dt \tag{2.2}$$

2.3 Reduced Order Model

2.3.1 Methodology

A generalized WEC is assumed for the presented study: the Reference Model 3 (RM3) two-body point absorber [14]. The geometry of the RM3 WEC is shown in Fig. 2.1. It consists of two parts: a central spar and a concentric float. The power take-off system (PTO) is placed between the float and the spar, to control the relative motion characteristics and hence, energy extraction of the system. In general, a given rigid object with no constraints has 6 degrees of freedom (DOF), which means it is free to move and rotate in 6 primary directions. The 6 DOF consists of 3 translational and three rotational. Because the RM3 system has two parts, it inherently has 12 DOF (2×6).

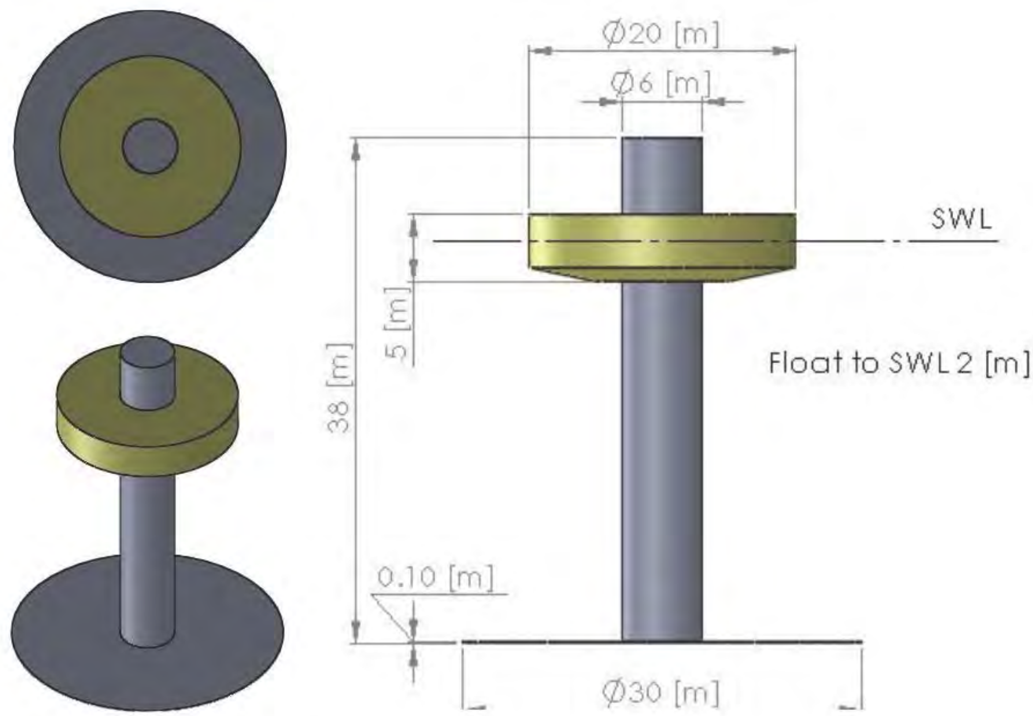

Figure 2.1: RM3 point absorber WEC geometry.

2.3.2 Constraints

Newton's second law of motion can be formulated for each of the degrees of freedom, which, in vector form: $\mathbf{m}\,\ddot{\mathbf{x}} = \mathbf{F}$ In this equation, $\mathbf{m}$ represents the mass matrix for all DOF (3 lumped masses and three mass moments of inertia), $\ddot{\mathbf{x}}$ is the acceleration of the mass system in all DOF, and finally, $\mathbf{F}$ represents the forces acting on the body. For instance, if one wants to develop the equation of motion for one of the bodies in RM3, float, for example, it becomes:

$$\begin{bmatrix} M_{11} & 0 & 0 & 0 & 0 & 0 \\ 0 & M_{22} & 0 & 0 & 0 & 0 \\ 0 & 0 & M_{33} & 0 & 0 & 0 \\ 0 & 0 & 0 & I_{xx} & 0 & 0 \\ 0 & 0 & 0 & 0 & I_{yy} & 0 \\ 0 & 0 & 0 & 0 & 0 & I_{zz} \end{bmatrix} \begin{bmatrix} \ddot{x}_1 \\ \ddot{x}_2 \\ \ddot{x}_3 \\ \ddot{x}_4 \\ \ddot{x}_5 \\ \ddot{x}_6 \end{bmatrix} = \begin{bmatrix} f_1 \\ f_2 \\ f_3 \\ f_4 \\ f_5 \\ f_6 \end{bmatrix}$$

In this vector equation, since the mass of the float is homogeneous, $M_{11} = M_{22} = M_{33} = M_{float}$; and f_i represents the total forcing terms acting on the i^{th} DOF.

Considering the two bodies in the RM3, if the bodies have no geometric constraints with respect to each other, then there would be 12 independent DOF. A system of 12 equations and 12 unknowns can then be set up and solved at each time step. However, the existing configuration has a geometric constraint between the spar and the float, allowing only an independent translational motion in heave. The RM3 configuration is in a way that the spar constrains all DOF of the float, except heave. Therefore there are 5 DOF constrained between float and spar (surge, sway, roll, pitch, and yaw) and 2 unconstrained DOF (heave of the spar and relative heave of the float with respect to spar), as depicted in Fig. 2. To address this reduction in the number of DOF, a constraint matrix is developed to map the responses (here, for example, displacements) from 12 DOF to 7 as $\mathbf{x} = \mathbf{T}_\mathrm{c}\mathbf{x}_\mathrm{c}$, in which, $\mathbf{x}$ is the displacement in 12 DOF of the two bodies, $\mathbf{T}_\mathrm{c}$ represents the constraint transformation, and $\mathbf{x}_\mathrm{c}$ is the resultant displacement in

7 DOF after constraint. If the initial distance between the centers of gravity of float and spar is denoted by d and assumes small rotation angles in pitch and roll ($\cos\phi = 1$ and $\sin\phi = \phi$), then we can derive the linear simplified geometrical constraint transformation as:

$$\begin{bmatrix} x_{1f} \\ x_{2f} \\ x_{3f} \\ x_{4f} \\ x_{5f} \\ x_{6f} \\ x_{1s} \\ x_{2s} \\ x_{3s} \\ x_{4s} \\ x_{5s} \\ x_{6s} \end{bmatrix} = \begin{bmatrix} 1 & 0 & 0 & 0 & d & 0 & 0 \\ 0 & 1 & 0 & d & 0 & 0 & 0 \\ 0 & 0 & 1 & 0 & 0 & 0 & 1 \\ 0 & 0 & 0 & 1 & 0 & 0 & 0 \\ 0 & 0 & 0 & 0 & 1 & 0 & 0 \\ 0 & 0 & 0 & 0 & 0 & 1 & 0 \\ 1 & 0 & 0 & 0 & 0 & 0 & 0 \\ 0 & 1 & 0 & 0 & 0 & 0 & 0 \\ 0 & 0 & 1 & 0 & 0 & 0 & 0 \\ 0 & 0 & 0 & 1 & 0 & 0 & 0 \\ 0 & 0 & 0 & 0 & 1 & 0 & 0 \\ 0 & 0 & 0 & 0 & 0 & 1 & 0 \end{bmatrix} \begin{bmatrix} x_{1s} \\ x_{2s} \\ x_{3s} \\ x_{4s} \\ x_{5s} \\ x_{6s} \\ x_7' \end{bmatrix}$$

In this matrix, variables x_{1f} through x_{6f} represent the 6 DOF of the float (surge, sway, heave, roll, pitch, yaw), and x_{1s} through x_{6s} are the 6 DOF of the spar. The 6 variables on the right-hand side of the equation are defined at the center of gravity of the spar in addition to x_7' representing the relative heave displacement at the center of gravity of the float. In the constrained DOF, both the float and the spar have the same accelerations, velocities, and displacements. The

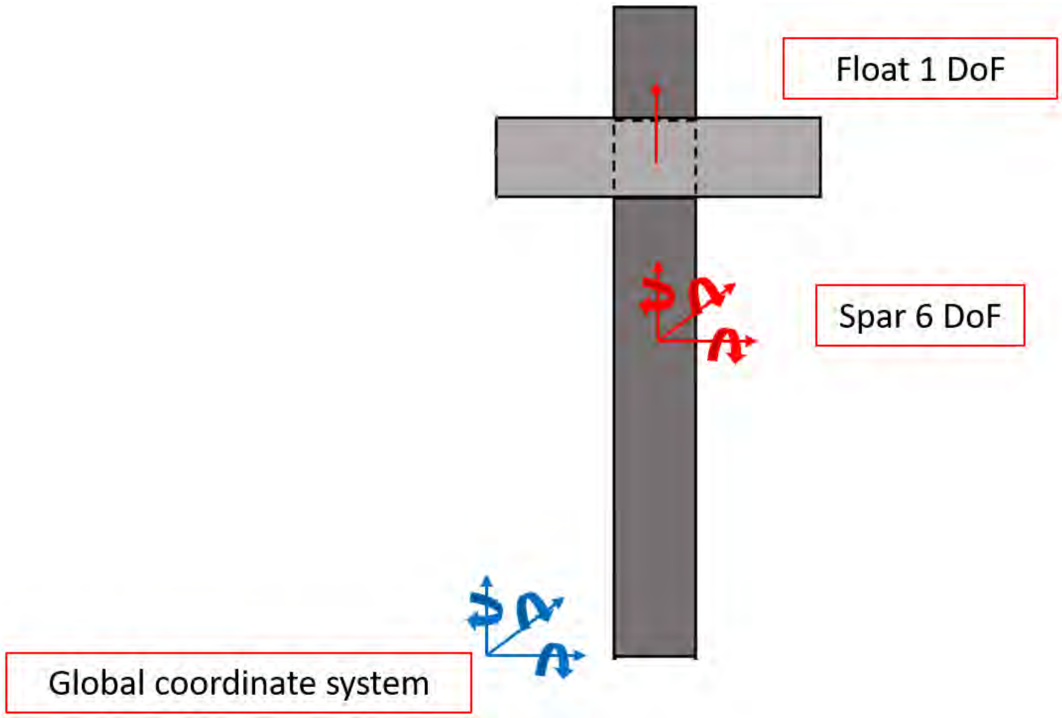

Figure 2.2: Degrees of freedom and local/global (red/blue) coordinate system definition for the RM3 WEC.

constraint reduces the total number of DOF from 12 to 7, assuming 7 of them at the center of gravity of the spar ($\ddot{x}_{1s}, \ddot{x}_{2s}, \ldots, \ddot{x}_{6s}$) and the relative motion ($\ddot{x}_7'$) at the center of gravity of the float. The original 12 by 12 matrices are constructed from wave analysis in Massachusetts Institute of Technology hydrodynamic coefficient outputs and reduced down to 7 by 7 using the constraint transformation matrix $\mathbf{T}_\mathrm{c}$ introduced above as $\mathbf{M}_\mathrm{c} = \mathbf{T}_\mathrm{c}^\top \mathbf{M} \mathbf{T}_\mathrm{c}$, $\mathbf{B}_\mathrm{c} = \mathbf{T}_\mathrm{c}^\top \mathbf{B} \mathbf{T}_\mathrm{c}$, $\mathbf{K}_\mathrm{c} = \mathbf{T}_\mathrm{c}^\top \mathbf{K} \mathbf{T}_\mathrm{c}$, and $\mathbf{F}_\mathrm{ex} = \mathbf{T}_\mathrm{c}^\top \mathbf{F}_\mathrm{c}$, where $\mathbf{M}_\mathrm{c}$, $\mathbf{B}_\mathrm{c}$, and $\mathbf{K}_\mathrm{c}$ are the constrained mass, damping, and stiffness matrices, respectively. This results in seven equations and seven unknowns: $\mathbf{M}_\mathrm{c}\ddot{\mathbf{x}}_\mathrm{c} + \mathbf{B}_\mathrm{c}\dot{\mathbf{x}}_\mathrm{c} + \mathbf{K}_\mathrm{c}\mathbf{x}_\mathrm{c} = \mathbf{F}_\mathrm{c}$.

All the hydrodynamic coefficients from wave analysis in Massachusetts Institute of Technology are computed relative to the local axis of each body, assuming gravitational acceleration pointing straight downward. Since the location and orientation of each body change in time, we need to transfer all the hydrodynamic matrices into global coordinates using Euler Angle Transformations (roll (ϕ), pitch (θ), and yaw (ψ)) which decomposes the body-fixed variables to global coordinate. In general: $\mathbf{u}_g = \mathbf{T} \times \mathbf{u}_l$, in which, $\mathbf{u}_g$ and $\mathbf{u}_l$ are the variables in global and local coordinates, respectively, and $\mathbf{T}$ is the transformation matrix. In the presented study, since originally the rotations are assumed to be small, then the $\mathbf{T}$ matrix is unity, and global and local coordinates are assumed to be the same.

2.3.3 Basis and Assumptions for Modal Analysis

The modal analysis of the 7 DOF system results in 7 natural frequencies of the structure (WEC) and 7 Eigenvectors. Because the WEC is symmetric and the wave field is assumed long crested (no variation in y-direction), it can be assumed that all the WEC responses are in the 2D plane of x-z. Given the fact that every combination of variables can be described in a 2D plane with 2 orthogonal vectors, 2 modes were chosen out of the 7 modes resulting from the modal analysis of the system. The procedure to choose the 2 modes incorporates the assumption that the most important driving force in the system is the excitation force from the incoming waves. Hence, the two modes with frequencies closest to the incoming waves frequencies were selected, and the corresponding Eigenvectors $\mathbf{\Phi}_{\mathrm{m}} = [\mathbf{\Phi}_1 \mathbf{\Phi}_2]$

are used to reduce the system to 2 DOF in Eigen domain using the Eigenvectors $\mathbf{\Phi}_m$ as $\mathbf{\Phi}_m^T\mathbf{M}_c\mathbf{\Phi}_m = \mathbf{M_e}$, $\mathbf{\Phi}_m^T\mathbf{B}_c\mathbf{\Phi}_m = \mathbf{B_e}$, $\mathbf{\Phi}_m^T\mathbf{K}_c\mathbf{\Phi}_m = \mathbf{K}_{\mathrm{e}}$, and $\mathbf{\Phi}_m^T\mathbf{F}_c = \mathbf{F}_{\mathrm{e}}$, in which $\mathbf{M}_{\mathrm{e}}$, $\mathbf{B}_{\mathrm{e}}$, $\mathbf{K}_{\mathrm{e}}$, and $\mathbf{F}_{\mathrm{e}}$ represent the 2 DOF equivalent variables in the Eigen domain. Finally, the reduced order equation of motion becomes:

$$\underbrace{\begin{bmatrix} F_{e_1}(t) \\ F_{e_2}(t) \end{bmatrix}}_{\Phi_m^T F_{exc}} = \underbrace{\begin{bmatrix} m_{11} & m_{12} \\ m_{21} & m_{22} \end{bmatrix}}_{\Phi_m^T M_c \Phi_m} \begin{bmatrix} \ddot{x}_{e_1}(t) \\ \ddot{x}_{e_2}(t) \end{bmatrix} + \underbrace{\begin{bmatrix} b_{11} & b_{12} \\ b_{21} & b_{22} \end{bmatrix}}_{\Phi_m^T B_c \Phi_m} \begin{bmatrix} \dot{x}_{e_1}(t) \\ \dot{x}_{e_2}(t) \end{bmatrix} + \underbrace{\begin{bmatrix} k_{11} & k_{12} \\ k_{21} & k_{22} \end{bmatrix}}_{\Phi_m^T K_c \Phi_m} \begin{bmatrix} x_{e_1}(t) \\ x_{e_2}(t) \end{bmatrix} \quad (2.3)$$

in which, the accelerations/velocities/displacements are in the Φ_1, Φ_2 basis, instead of the original DOF. The computed response quantities can be transformed back to the 7 DOF system by inverting the process of the reduction.

The frequency range for this analysis was selected based on the assumption of heave-dominated WEC behavior. As it can be seen from Fig.2.3, for float and spar, when investigating the excitation coefficients, one can find the transition period for the heave-dominated motion is about 5.2 s for float and spar. To this end, the range of periods included in the presented study was limited to a minimum of 5 seconds.

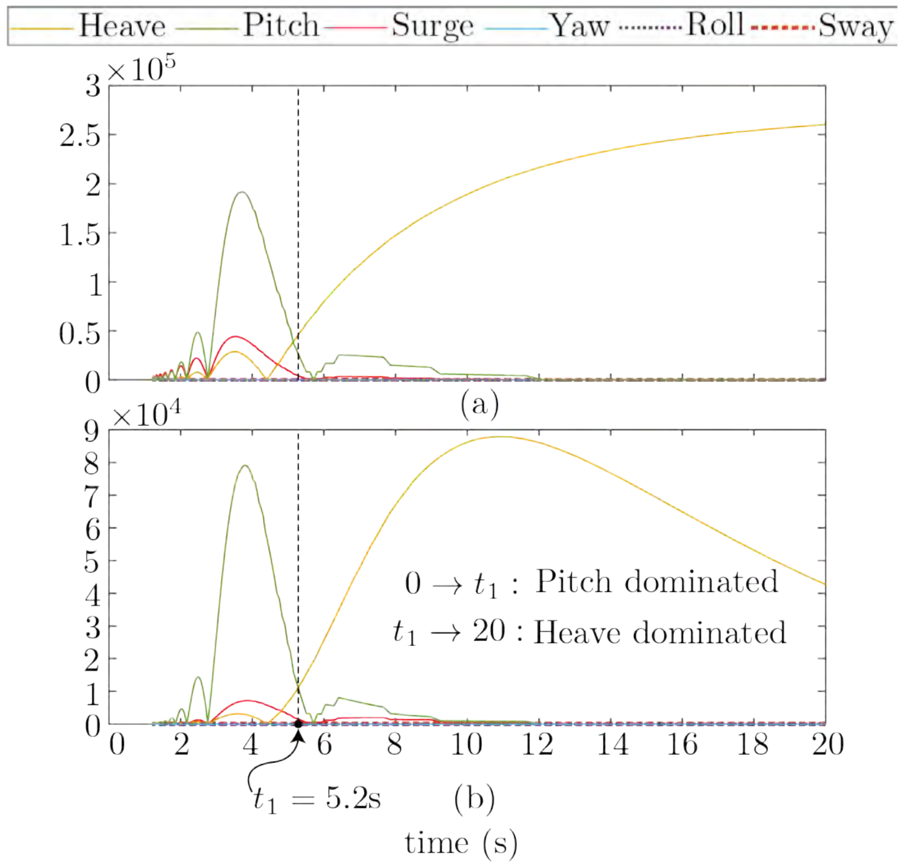

Figure 2.3: RM3 excitation force coefficients for (a) float (b) spar for all 6 DOF as a function of excitation period. For low periods, pitch dominates, and at large periods, heave dominates.

2.3.4 ROM Validation via Comparison to WEC-Sim

The general assumptions that are included in the simulation validation runs, compared to WEC-Sim results, are (1) the duration and ramp time for simulations in both ROM and WEC-Sim models were chosen as 100 and 20 wave periods (peak period for irregular waves); (2) time step was fixed at 0.01 s for both ROM and WEC-Sim models; (3) for regular and irregular waves, the period range of 5 s to

13 s seconds were included in the simulation due to heave dominancy; (4) for irregular waves, a JONSWAP spectrum with equal energy assumption was used in WEC-Sim, with specified range of periods between 4 and 20 seconds, to include the developing sea-states for higher energetic conditions. The error definition was defined as the difference between the results from ROM with those generated by WEC-Sim in the following manner:

- The measure of the error for regular waves is assumed as the percent difference between the amplitude of response in heave.

$$\text{Error}_{\text{regular}} = 100 \times \frac{H_{\text{ROM}} - H_{\text{WEC-Sim}}}{H_{\text{WEC-Sim}}}$$

- The measure of the error for irregular waves is assumed as the percent difference between the standard deviations of the heave response.

$$\text{Error}_{\text{irregular}} = 100 \times \frac{\sigma_{\text{ROM}} - \sigma_{\text{WEC-Sim}}}{\sigma_{\text{WEC-Sim}}}$$

- For irregular waves, each peak period was modeled 10 times with random phases, and the mean value is reported as the mean error.

$$\text{Mean Error}_{\text{irregular}} = \frac{\sum_{i=1}^{10} \text{Error}_{\text{irregular}}\ (i)}{10}.$$

The analysis of the RM3 WEC was performed using the proposed ROM model and WEC-Sim, and the results were compared. It should be mentioned that in

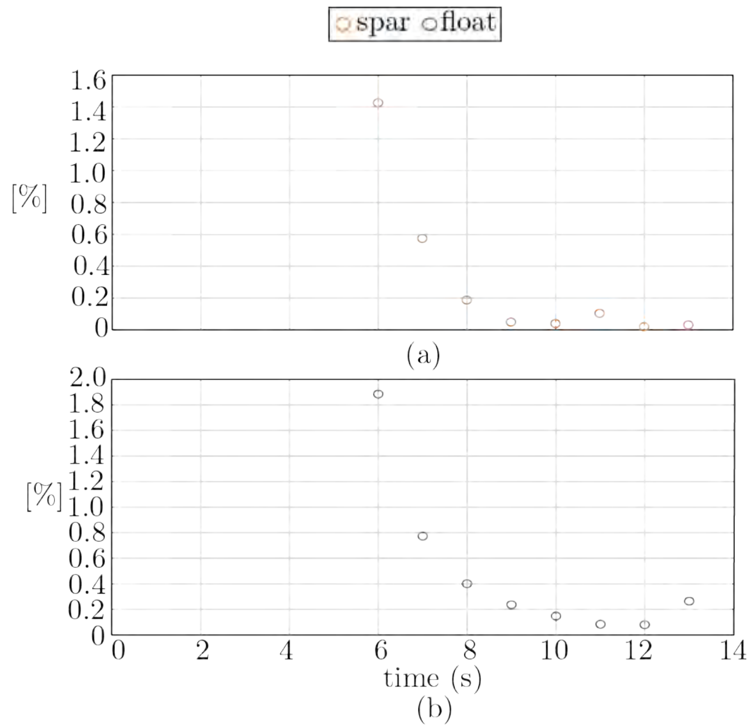

Figure 2.4: Maximum amplitude difference between the Reduced Order Model and WEC-Sim for regular waves for (a) spar and (b) float.

WEC-Sim analysis, none of the "nonlinear" features of the program were enabled. The range of periods considered is 5 s to 13 s with a constant wave height of 1 m, with PTO damping of zero.

Calculated errors as outlined previously are presented in Fig.2.4(a) and Fig.2.4(b) for the float and spar, respectively. From the figures, it can be found that the difference between ROM and WEC-Sim results stays below 5 %. Also, the maximum error occurs at a period of 5 s which, as explained previously, is not considered in the heave-dominated region and does not completely satisfy the small rotation assumption of the presented ROM model.

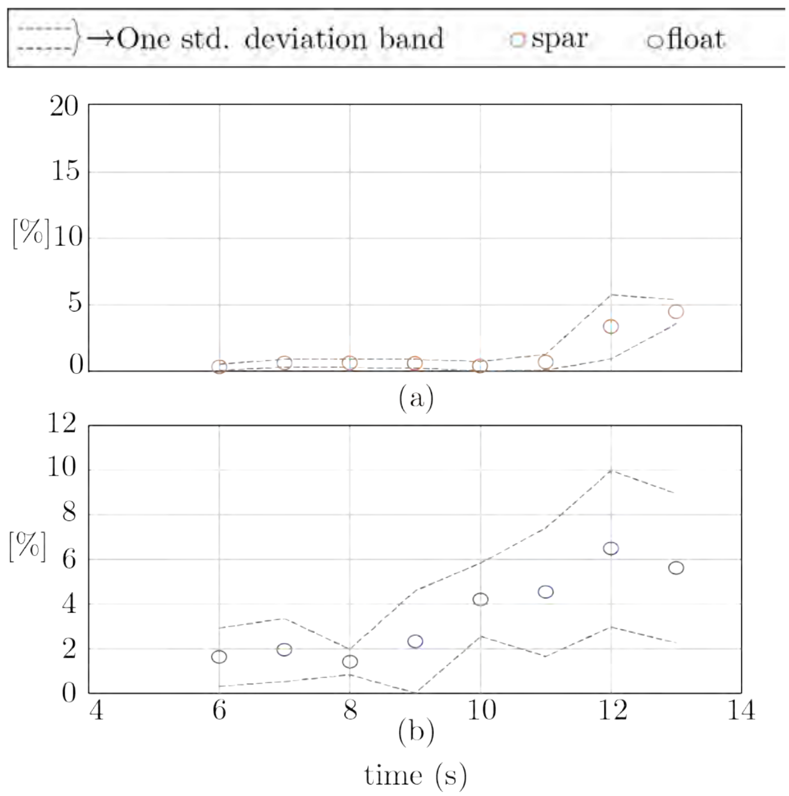

Figure 2.5: Mean standard deviation difference between the Reduced Order Model and WEC-Sim for irregular Waves for (a) spar and (b) float. (The dashed line represents one standard deviation band.)

The same analysis was performed under irregular wave conditions with a range of peak period of $T_p = 5$ s to 13 s and significant wave height of $H_s = 1$ m, following a Joint North Sea Wave Project (JONSWAP) spectrum with $\gamma = 1$ and PTO damping of zero [7]. The wave field for each wave condition was generated 10 times with random phases for both ROM and WEC-Sim models, and errors were computed using the definition mentioned previously. Calculated mean errors with upper and lower bounds of one standard deviation also are presented in Fig. 2.5 (a) and Fig. 2.5 (b) for the float and spar, respectively. Fig. 2.5 (a) shows a large mean error for $T_p = 5$ s caused by large rotation contributions from periods smaller than 5.2 s. For the rest of the test cases, the difference between ROM and WEC-Sim results remains below 5 %.

2.3.5 Circuit Representation of ROM

The two second-order differential equations in (3.1) are modeled as two isolated circuits by Equation (2.2), with the assumption that all the coefficient matrices are diagonalized by Eigen-decomposition. As a result, the non-diagonal components in the mass matrix and K matrix are close to zero. However, the non-diagonal components in the damping matrix have significant values due to the electromagnetic damping from the PTO unit. To address the coupling terms b_{12} and b_{21} in (3.1), a gyrator is introduced, converting the voltage of the neighbor circuit to the current with a gyration ratio of $G = b_{12}$. Notably, $b_{12} \approx b_{21}$ is due to Newton's third law. The schematic of the Equivalent circuit is described in Fig. 2.6.

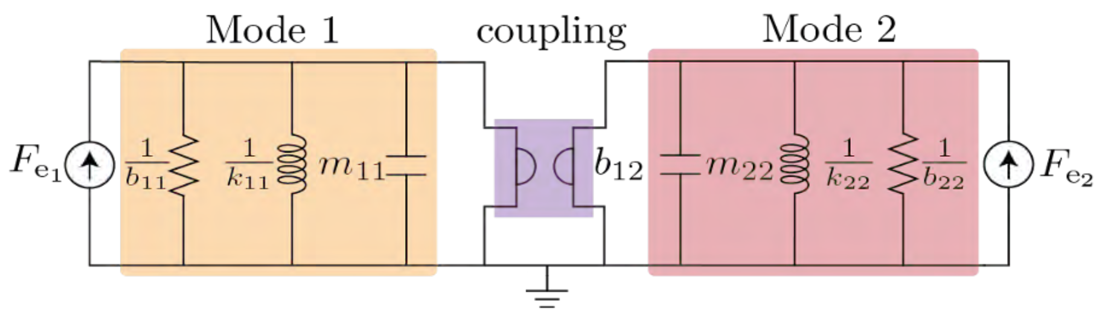

Figure 2.6: Equivalent circuit schematic in which each of the two coupled circuit components represents the two dominant modes of RM3 relative motion.

2.4 Irregular Wave Case

In this paper, regular waves and irregular waves are subjected as input to the equivalent circuit model. A regular wave is defined as a wave with constant amplitude and a constant time period between crests. The irregular wave is created using the JONSWAP spectrum [7] with significant wave height and dominant frequency as depicted in Table 2.2. Both wave elevation profiles were converted into excitation force time series using the boundary element method for input-output analysis. Since the regular waves have a single frequency, the hydrodynamic coefficients are constant. On the other hand, the frequency of the incoming wave fluctuates over time in irregular wave cases. Since the hydrodynamics coefficients are dependent on the frequency of the incoming wave, WEC-Sim solves the problem by calculating the convolution with the impulse response function of each coefficient, which is derived from the frequency domain analysis.

2.4.1 Fixed Frequency Model

The fixed frequency equivalent circuit model (FFM) assumes the wave input can be modeled as a single constant frequency, and therefore the components of the equivalent circuit model are constant and can be modeled as simple passive circuit components (resistors, capacitors, etc.)

2.4.2 Instantaneous Frequency Model

In contrast to the Fixed Frequency Model, an Instantaneous Frequency Model (IFM) uses constant circuit parameters, but the parameters are updated at each sample time according to an estimated instantaneous excitation frequency.

Through linear random wave theory, the analytic expression $x(t)$ of the wave time series generated from the JONSWAP spectrum with $\gamma = 1$ can be expressed as

$$x(t) = A(t)\cos\left(\overline{w}t + \epsilon(t)\right) \tag{2.4}$$

in which $\epsilon(t)$ represents a slowly varying phase information, $\overline{w}$, which is the energy mean angular frequency of the spectrum, and $A(t)$ is a function of the slowly varying envelope amplitude of the wave, which follows a Rayleigh distribution [11]. To estimate the instantaneous frequency of the wave excitation signal, the instantaneous phase of $x(t)$ can be defined as $\chi(t) = \arg(x_{\mathrm{a}}(t)) = \arg(x(t) + j\hat{x}(t))$, where $x_{\mathrm{a}}(t)$ denotes the analytic representation of $x(t)$, and $\hat{x}(t)$ is the Hilbert Transform of $x(t)$ [3]. The analytic representation with the Hilbert Transformed signal can be expressed as $x_a(t) = A(t)e^{j(\overline{w}t+\epsilon(t))}$, therefore, $\chi(t) = \overline{w}t + \epsilon(t)$.

By differentiating $\chi(t)$, the analytic instantaneous frequency

$$\dot{\chi}(t) = \overline{w} + \dot{\epsilon}(t) \tag{2.5}$$

is obtained, in which $\overline{w} = \frac{m_1}{m_0}$ (m_1 and m_0 are the first and zeroth-order spectral moments of the JONSWAP spectrum) and $\dot{\epsilon}(t)$ is relatively small and slowly varying.

In the discrete-time domain, $\hat{x}[n]$ can be approximated by the discrete Hilbert transform of $x[n]$ via Discrete Time Fourier Transform (DTFT), expressed as $\hat{x}[n] \approx \mathcal{H}[x[n]]$, due to the slow varying nature of $A(t)$ and $\epsilon(t)$. As a result, $\chi[n] = \arctan\left(\frac{\mathcal{H}[x[n]]}{x[n]}\right)$ is obtained. By differentiating $\chi[n]$, the instantaneous frequency is obtained

$$\dot{\chi}[n] = \{\arctan\left(\frac{\mathcal{H}[x[n]]}{x[n]}\right) - \arctan\left(\frac{\mathcal{H}[x[n-1]]}{x[n-1]}\right)\}\frac{1}{\Delta t} \tag{2.6}$$

However, the differentiation and DTFT operation can result in noise amplification and large transients, so a moving average filter is usually applied. The filter window size is estimated as ten times the model period (energy peak period) in the power spectrum density function as shown in Fig. 3.2(c). An example of the instantaneous frequency along with the corresponding wave data are presented in Fig. 3.2(a) and Fig. 3.2(b). The $\overline{w}$ expressed in Hz is presented in Fig. 3.2(c), which shows the average of the estimated instantaneous frequency is close to the analytic instantaneous frequency as expected.

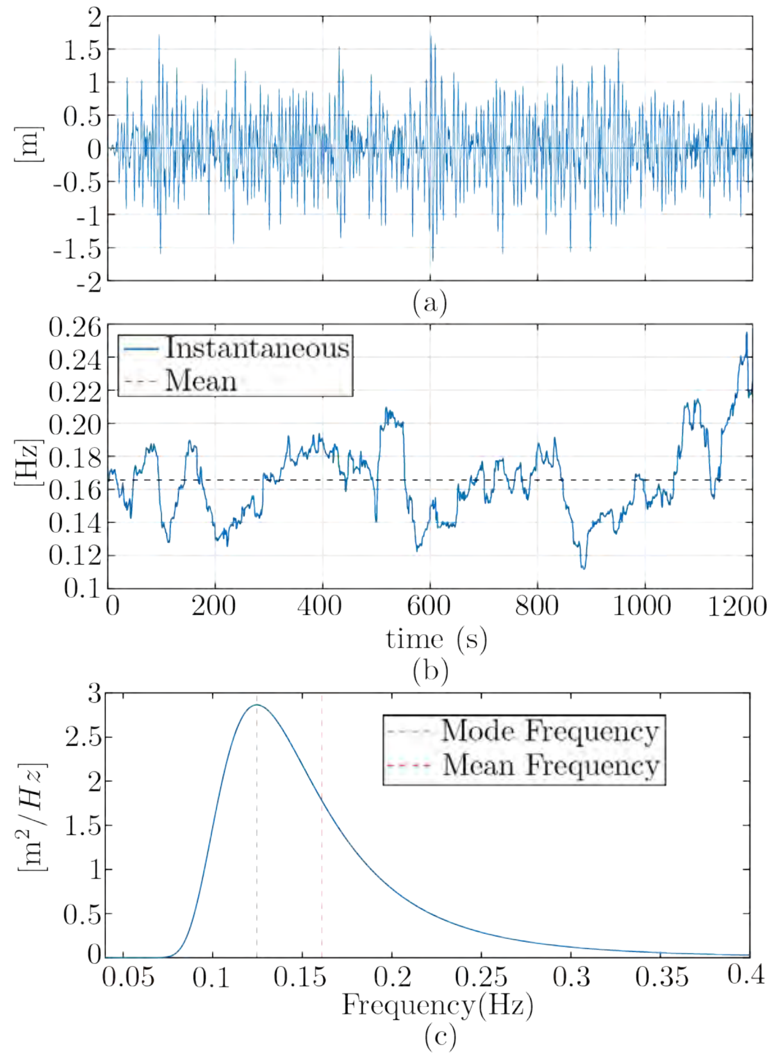

Figure 2.7: (a) Water surface elevation; (b) instantaneous frequency; (c) power spectrum density. The mean frequency is 0.1614 Hz and the computed energy mean from the PSD is 0.1657 Hz.

2.5 Simulation Results

A regular case is simulated with parameters shown in Table 2.2 using WEC-Sim and the equivalent circuit model.

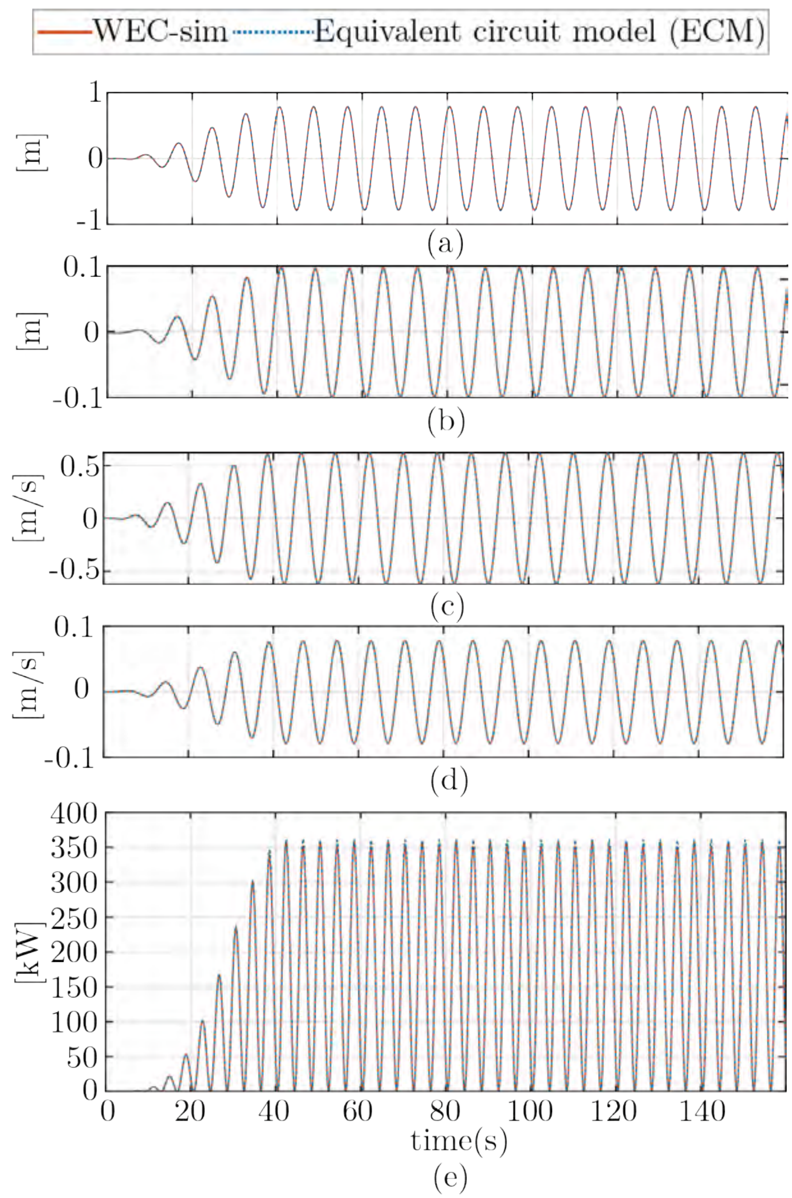

Figure 2.8: (a) Float and (b) spar displacement; (c) float and (d) spar velocity; (e) PTO power for the regular wave case.

The irregular cases generated from WEC-Sim exhibit randomness in the time domain due to the phase information. This randomness introduces variations in the

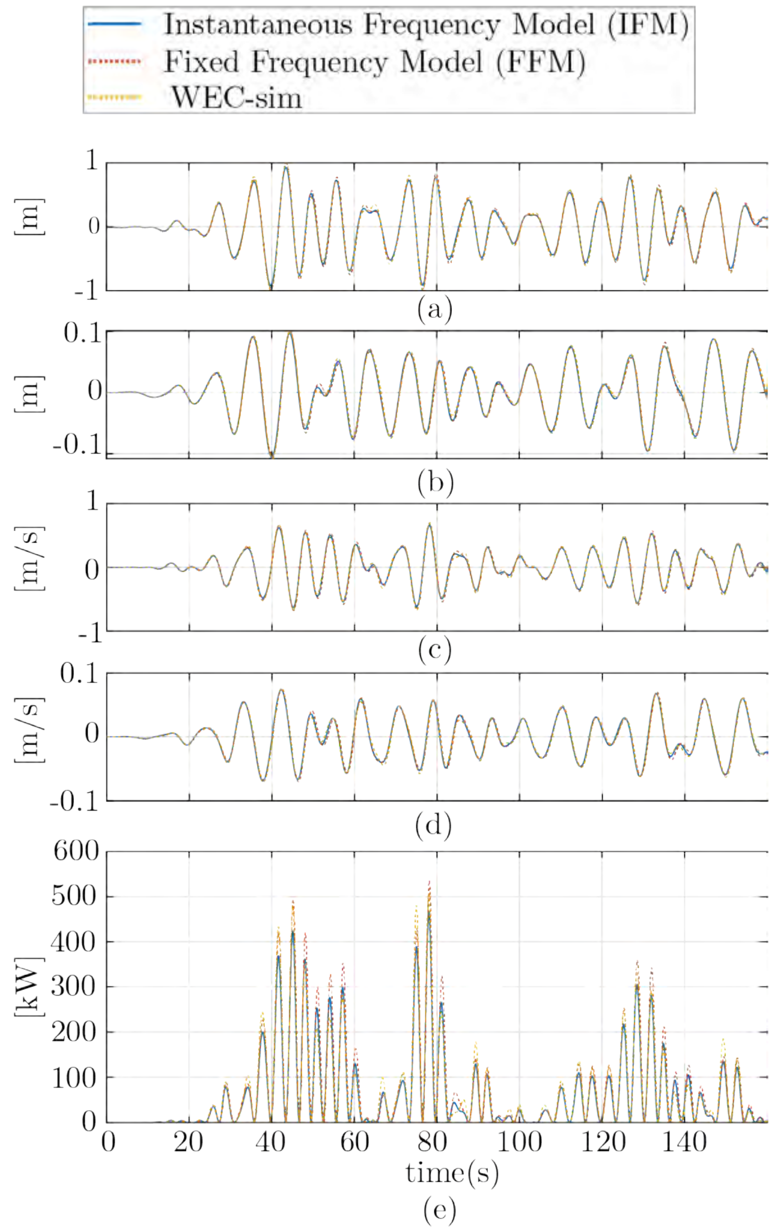

Figure 2.9: (a) Float and (b) spar displacement; (c) float and (d) spar velocity; (e) PTO power for the irregular wave case.

Table 2.2: Simulation Parameters

Parameters	**Regular**	**Irregular**
Wave height	2 m	
Wave Frequency	0.125 Hz	
Duration	1200 s	
Timestep	0.1 s	
Ramptime	40 s	
PTO damping	1200000 Ns/m	

simulation results, which can lead to both larger and smaller errors between WEC-Sim and the equivalent circuit model. The variations in the phase information can cause the models to produce slightly different responses, resulting in varying degrees of error between the two simulations. To address the issue, the ten irregular wave cases, which share the same PSD of waves, were simulated using WEC-Sim, FFM, and IFM with the simulation parameters described in Table 2.2. A ramp function, which allows the excitation force to fully develop at a set time, was used to mitigate transient issues. The PTO unit was assumed to be a simple damper.

- Root-Mean-Squared-Errors (RMSE) were calculated by subtracting the values between the two simulations at each time step. The RMSEs are normalized by the Root-Mean-Squared values of WEC-Sim responses.

$$\mathrm{Error}_{\mathrm{RMSE}} = 100 \times \frac{\mathrm{Mean}(\sqrt{\Sigma(X_{\mathrm{model}} - X_{\text{WEC-Sim}})^2})}{\mathrm{Mean}(\sqrt{\Sigma(X_{\text{WEC-Sim}})^2})}$$

The simulation results of the equivalent circuit model closely match WEC-Sim's responses in regular wave cases within 3% error as shown in Table 2.3. Figure 2.8 shows the simulation results of the equivalent circuit model compared with WEC-

Sim for the first 160 seconds in a regular wave case. The values in Table 2.4 represent the average errors from ten different irregular wave cases.

Table 2.3: Errors in Regular Case

Variables	**float**	**spar**
Displacement	0.8%	2.04%
Velocity	0.85%	1.54%
Power generation	1.71%	

Table 2.4: Errors in Irregular Cases

	IFM		**FFM**	
Variables	**float**	**spar**	**float**	**spar**
Displacement	10.2%	10.7%	11.0%	9.4%
Velocity	10.2%	11.2%	14.5%	12.4%
Power generation	15.51%		21.0%	

The IFM exhibits slightly better overall results compared to FFM, except for the displacement in the spar. Figure 2.9 presents an example of results from WEC-Sim, FFM, and IFM for 160 seconds. The simulations were conducted on a MacBook Pro 16 (2021 model). The total elapsed times were measured for each model to simulate the ten irregular wave cases. The elapsed times for each model are as follows:

- FFM: 14.6 seconds
- IFM: 26.0 seconds
- WEC-Sim: 94.8 seconds

And the comparison of the elapsed times relative to WEC-Sim:

$$\begin{aligned}
\text{FFM is} \quad & \frac{94.8\,\text{seconds}}{14.6\,\text{seconds}} \approx 6.49\,\text{times faster than WEC-Sim.} \\
\text{IFM is} \quad & \frac{94.8\,\text{seconds}}{26.0\,\text{seconds}} \approx 3.65\,\text{times faster than WEC-Sim.} \\
\text{FFM is} \quad & \frac{26.0\,\text{seconds}}{14.6\,\text{seconds}} \approx 1.78\,\text{times faster than IFM.}
\end{aligned}$$

2.6 Conclusion

The equivalent circuit of the Reduced Order Model, obtained through modal analysis, exhibits the potential for simplicity in PTO control optimization via energy-focused DOF reduction. Additionally, this concise representation significantly reduces computational costs, enabling real-time control of the PTO unit with reduced delays. The paper not only offers a structural analysis of RM3 supporting the DOF reduction but also introduces a novel approach to estimating the instantaneous frequency and its corresponding modeling for real sea conditions. This modeling technique will be valuable for future research in developing equivalent circuit models for Wave Energy Converters, facilitating more accurate simulations under real sea conditions. The equivalent circuit model of RM3 via Eigen analysis is simulated and compared with WEC-Sim. The equivalent circuit model performs exceptionally well in regular wave cases. The Instantaneous Frequency Model (IFM) performs well in calculating the response of RM3 bodies, while the Fixed Frequency Model (FFM) demonstrates computational advantages in irregular wave cases. However, the primary objective of the circuit representation is to optimize the Power Take-Off (PTO) unit control. Given that the error in power generation is around 4.5% lower in IFM, the IFM would be a more reliable model for PTO control optimization. Future research will focus on using the IFM to improve performance in impedance matching control. Additionally, experimental validation of the models is in progress with Laboratory Upgraded Point Absorber (LUPA), an open-source two-body point absorber wave energy converter, built and tested at Oregon State University [1]. The LUPA specification is shown in Fig. 2.10.

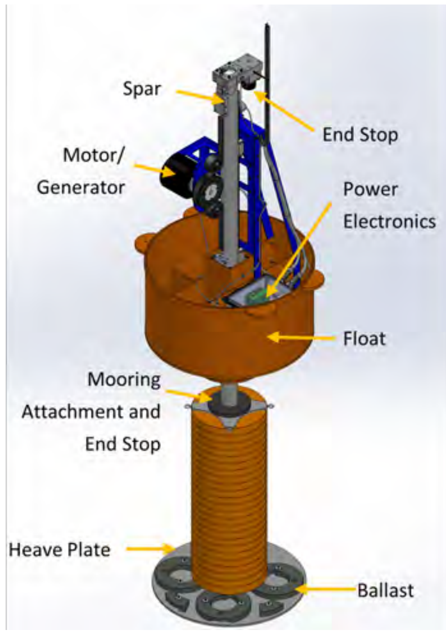

(a)

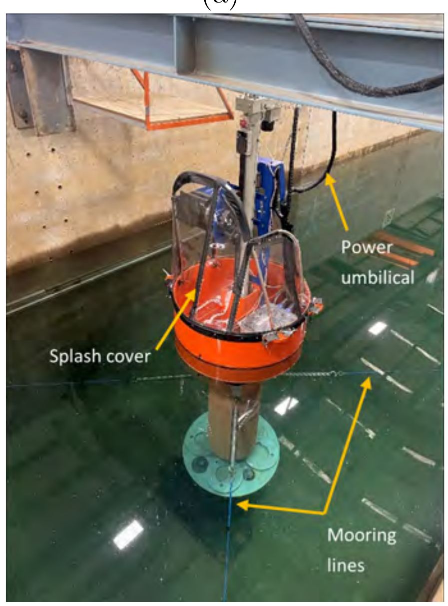

(b)

Figure 2.10: (a) LUPA schematic and (b) experimental testing at the O.H. Hinsdale Wave Laboratory at Oregon State University.

Chapter 3: Manuscript 2

3.1 Introduction

In this study, we undertake a comprehensive analysis of a 2-body wave energy converter (WEC) using a reduced-order model (ROM) derived through Eigen analysis. For validation, the ROM model results are compared against WEC-Sim, a widely recognized WEC numerical modeling tool [14]. Our analysis focuses on the Representative Model 3 (RM3) within WEC-Sim. The reduced-order model enhances precision through equivalent circuit modeling. This equivalent circuit methodology holds the potential for optimal Power-Take-Off (PTO) unit control, employing the impedance matching technique. To optimize computational efficiency and minimize errors in field sea conditions relative to WEC-Sim, we introduce the instantaneous frequency of wave data into the equivalent circuit. Additionally, this novel modeling technique paves the way for potential control strategies due to its instantaneous characteristics. We present simulation results employing diverse control techniques using the equivalent circuit model, leveraging the instantaneous frequency of wave data.

3.2 Equivalent Circuit Modeling of a WEC via Eigen Analysis

3.2.1 Reduced Order Model

The presented study utilizes a generalized two-body point absorber, one of the standard configurations in NREL's WEC-Sim: the RM3 point absorber. It is made up of a Spar (central section) and a Float, with a Power Take-Off system (PTO) in between. The PTO controls the relative motion and determines energy extraction. Typically, a rigid body has 6 degrees of freedom (DOF), and given the RM3 has two parts, it possesses 12 DOF (2×6). Using Newton's second law, $m\ddot{x} = f$, one can determine the responses of the WEC given the forces acting on the bodies. The total force, $f(t)$, comprises excitation, radiation damping, forces from PTO, viscous effects, buoyancy and restoring, and mooring system forces. These forces' calculations use hydrodynamic coefficients obtained from WAMIT [10]. The configuration of RM3 has a set of geometric constraints between the spar and the float that only allows a relative translational motion of the float in heave respective to (w.r.t.) the spar. In this manner, there are a total of 7 dynamic DOF, 6 DOF defined at the CG of the spar and the 7th one, the relative heave motion of the CG of the float (w.r.t. the C.G. of the spar). Enforcing this constraint can be performed using a constraint matrix in the form of $x = T_c x_c$, where x is the displacement in 12 DOF of the two bodies, T_c represents the constraint matrix, and x_c the reduced DOF. The conference paper from authors in the process of publication on ECCE 2023 explains the details of T_c. The constraint reduces the total number of DOF from 12 to 7, for example, for the hydrodynamic coefficients using $T_c^T(H)T_c = H_c$, in which, H represents the hydrodynamic coefficients. The modal analysis of the 7 DOF system results in several modes of the structure (WEC) and 7 Eigenvectors. Since the problem in hand is symmetrical in space, in a way that the WEC itself is symmetrical and the wave field is assumed long crested (no variation in y-direction), it can be assumed that all the WEC responses are in the 2D plane of x-z and can be presented by 2 orthogonal vectors. Hence, 2 modes were chosen from the modal analysis of the system, the modes with frequencies closest to the incoming waves frequencies were selected, and the corresponding Eigenvectors, Φ_m, are used to reduce the system to 2 DOF in the Eigen domain, using for example $\Phi_m^T M_c \Phi_m = M_e$. In this expression, M_c represents the mass matrix and can be replaced by B_c, K_c, and F_c, as the radiation damping, stiffness, and forcing matrices. The right-hand side, M_e, is the 2 DOF equivalent variables in the Eigen domain. Finally, the reduced order equation of motion becomes:

$$\underbrace{\begin{bmatrix} F_{e_1}(t) \\ F_{e_2}(t) \end{bmatrix}}_{\Phi_m^T F_{exc}} = \underbrace{\begin{bmatrix} m_{11} & m_{12} \\ m_{21} & m_{22} \end{bmatrix}}_{\Phi_m^T M_c \Phi_m} \begin{bmatrix} \ddot{x}_{e_1}(t) \\ \ddot{x}_{e_2}(t) \end{bmatrix} + \underbrace{\begin{bmatrix} b_{11} & b_{12} \\ b_{21} & b_{22} \end{bmatrix}}_{\Phi_m^T B_c \Phi_m} \begin{bmatrix} \dot{x}_{e_1}(t) \\ \dot{x}_{e_2}(t) \end{bmatrix} + \underbrace{\begin{bmatrix} k_{11} & k_{12} \\ k_{21} & k_{22} \end{bmatrix}}_{\Phi_m^T K_c \Phi_m} \begin{bmatrix} x_{e_1}(t) \\ x_{e_2}(t) \end{bmatrix} \quad (3.1)$$

The analysis assumes a heave-dominated behavior for the WEC, with a transition period at around 5.2 s. Simulations used a time frame of 100 wave periods, with a time step of 0.01 s, using the JONSWAP spectrum for irregular wave simulations [7]. Errors are measured in amplitude difference and standard deviation difference for regular and irregular waves, respectively. Both regular and irregular wave results between ROM and WEC-Sim show a difference of under 5 %.

3.2.2 Modification on Constraint matrix

Several methods exist for defining a constraint matrix, including one that was described in the previous section. To accommodate various control algorithms and circuit representations, a modified constraint matrix was also formulated. In this modified version, the 7th DOF was specifically selected to represent the heave motion of the float. This choice contrasts with the original constraint matrix, where the 7th DOF was associated with the relative motion instead. The modified constraint matrix is critical in developing different equivalent circuit model strategies.

3.2.3 Equivalent Circuit Representation of Reduced Order Model

The relationship between forces and motion can be analogously linked to that of voltage and current. For instance, one can observe the same proportional relationships between $F = mdv/dt$ and the current-voltage relationship of a capacitor, $I = CdV/dt$. Through this analogy, we can draw parallels where force corresponds to current, mass equates to capacitance, and velocity corresponds to voltage. This analogy yields further relationships, as detailed in Table 1. Notably, even the control law of a generator and the force it produces, contingent on velocity or position, can be depicted as a circuit subsystem [2].

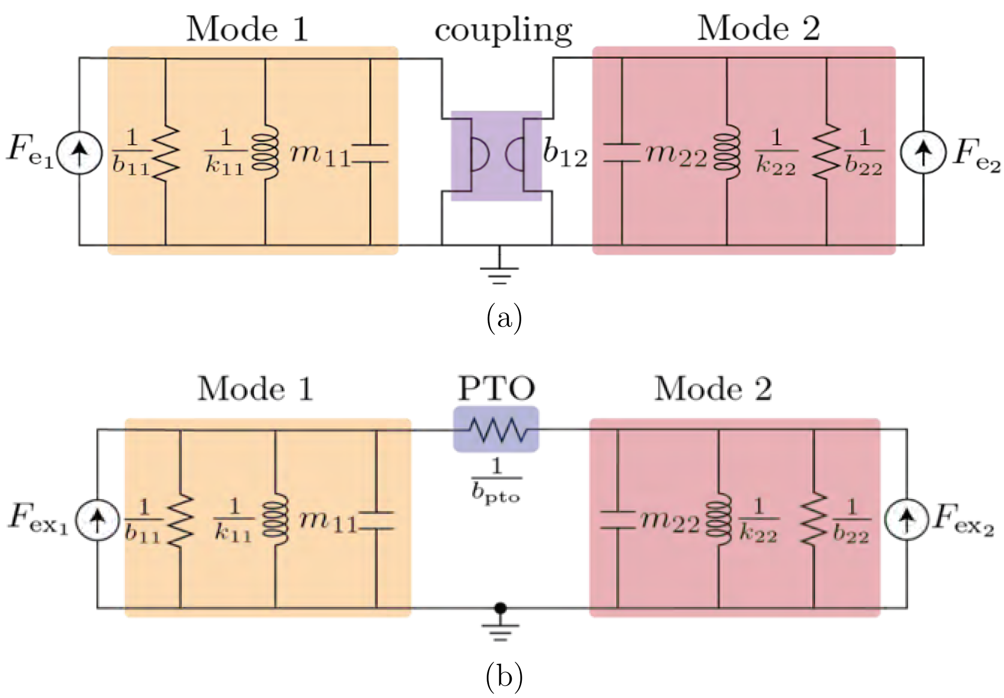

Figure 3.1: Schematics of RM3 equivalent circuits using (a) original constraint matrix and (b) modified constraint matrix respectively.

Note that non-diagonal terms, such as m_{12},m_{21},k_{12}, and k_{21} in equation 3.1, converge to zero due to the eigen decomposition performed during the brief diagonalization process. The reduced order equation 3.1 undergoes translation from its hydrodynamics terms to an equivalent circuit representation respectively, as demonstrated by the following equation:

$$I(t) = CV(t) + \frac{1}{R}V(t) + \frac{1}{L}\int V(t)dt \tag{3.2}$$

The equivalent circuit schematics of RM3, derived from two distinct constraint matrices, are presented in Fig.3.1 (a) and (b). Notably, the modified constraint matrix permits the placement of the PTO unit between the mode circuits, as depicted in Fig. (b). In contrast, the model employing the original constraint matrix necessitates dealing with coupled terms like b_{12} and b_{21}, making it challenging to identify a suitable location for the PTO unit within the circuit.

Table 3.1: Mechanical to Electrical Analogy

Mechanical	$\leftrightarrow$	**Electrical**
Force [N]	$\leftrightarrow$	Current [A]
Velocity [m/s]	$\leftrightarrow$	Voltage [Volts]
Mass [kg]	$\leftrightarrow$	Capacitance [F]
Damping [N/(m/s)]	$\leftrightarrow$	1/Resistance [1/Ohms]
Stiffness [N/m]	$\leftrightarrow$	1/Inductance [1/Henries]

3.3 Instantaneous Frequency Modeling

An instantaneous frequency model uses constant circuit parameters, but the parameters are updated at each sample time according to an estimated instantaneous excitation frequency. The analytic definition and derivation of the instantaneous frequency of wave data are shown in [8]. The discrete-time complex signal $x[n]$ can be approximated by the discrete Hilbert transform of the original signal $x[n]$ via the Discrete Time Fourier Transform (DTFT), expressed as $\hat{x}[n] \simeq \mathcal{H}[x[n]]$. As a result, the discrete-time instantaneous phase $\chi[n] = \arctan(\frac{\mathcal{H}[x[n]]}{x[n]})$ is obtained By differentiating $\chi[n]$, the discrete-time instantaneous frequency is obtained as

$$\dot{\chi}(t) = \{\arctan\left(\frac{\mathcal{H}[x[n]]}{x[n]}\right) - \arctan\left(\frac{\mathcal{H}[x[n-1]]}{x[n-1]}\right)\}\frac{1}{\Delta t} \tag{3.3}$$

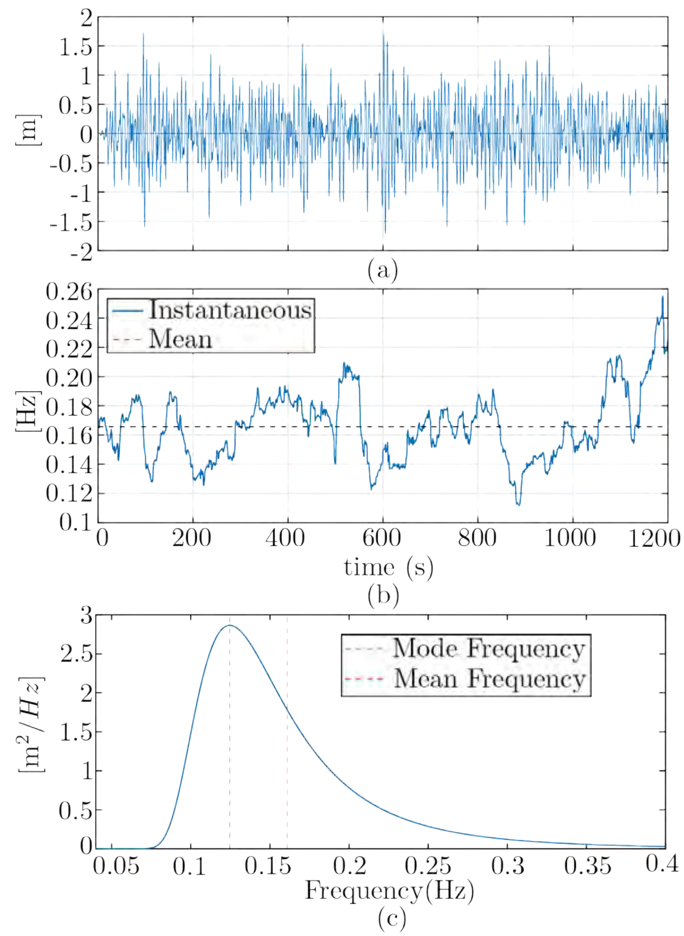

Figure 3.2: (a) Water surface elevation; (b) instantaneous frequency; (c) power spectrum density. The mean frequency is 0.1614 Hz and the computed energy mean from the PSD is 0.1657 Hz.

However, the differentiation and DTFT operation can result in noise amplification and large transients, so a moving average filter is usually applied. The filter

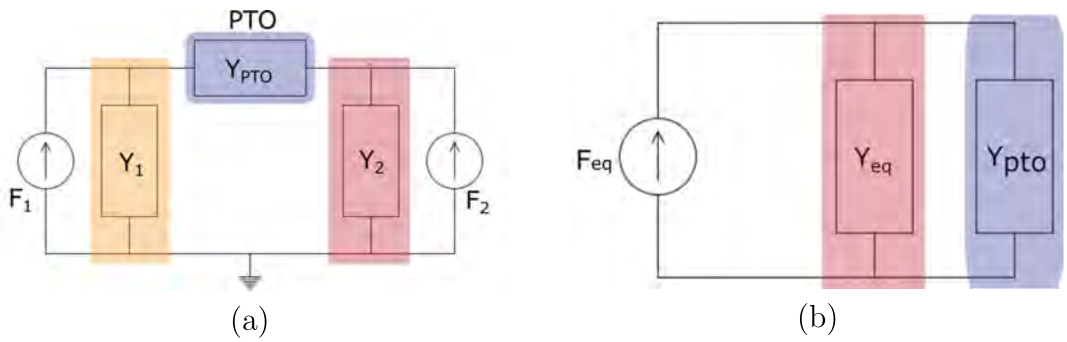

Figure 3.3: Schematics of (a) the abbreviated equivalent circuit and (b) Norton's Equivalent circuit

window size is estimated as ten times the model period (energy peak period) in the power spectrum density function as shown in Fig 3.2(c). An example of the instantaneous frequency along with the corresponding wave data is presented in Fig 3.2(a) and Fig 3.2(b). The $\bar{\omega}$ expressed in Hz is presented in Fig. 2(c), which shows the average of the estimated instantaneous frequency is close to the analytic instantaneous frequency as expected.

3.4 Impedance Matching Control Optimization

Let Y_1 and Y_2 be the admittances of individual modes, as depicted in Fig 3(a). The reduced-order model's equivalent circuit is transformed into a concise form, illustrated in Fig 3(b), using Norton's equivalent. The equivalent admittance is derived as $Y_{\mathrm{eq}}(\omega) = Y_1(\omega) \parallel Y_2(\omega)$ and), and the corresponding equivalent excitation force $F_{\mathrm{eq}}(\omega)$ is calculated as $F_{\mathrm{eq}}(\omega) = (F_1(\omega)Y_2(\omega) - F_2(\omega)Y_1(\omega))/(Y_1(\omega)+Y_2(\omega))$.

Moving forward, the complex PTO power

$$S_{\mathrm{pto}}(\omega) = P_{\mathrm{pto}}(\omega) + jQ_{\mathrm{pto}}(\omega) = |F_{\mathrm{eq}}(\omega)|^2/|Y_{\mathrm{eq}}(\omega) + Y_{\mathrm{pto}}(\omega)|^2 conj(Y_{\mathrm{pto}}(\omega))$$

is obtained. The real power in Equation 4 can be calculated as:

$$P_{\mathrm{pto}}(\omega) = v_{\mathrm{pto}}(\omega)F_{\mathrm{pto}}(\omega) = ((|F_{\mathrm{eq}}(\omega)|^2)/|Y_{\mathrm{eq}}(\omega) + Y_{\mathrm{pto}}(\omega)|^2)G_{\mathrm{pto}}(\omega)$$

in which $G_{\mathrm{pto}}(\omega)$ represents the real part of PTO admittance, equal to $real(Y_{\mathrm{pto}}(\omega))$. Note that $G_{\mathrm{pto}}(\omega)$ can be interpreted as the proportionality of velocity to force provided by the PTO, hence damping. The imaginary component of $Y_{\mathrm{pto}}(\omega)$ corresponds to the proportionality of acceleration or position to force. The optimization of PTO power generation occurs when $Y_{\mathrm{pto}} = Y^*_{\mathrm{eq}}$ since $F_{\mathrm{eq}}(\omega)$ and $Y_{\mathrm{eq}}(\omega)$ are determined and invariant in given wave conditions. However, achieving complex control of PTO is not always feasible, particularly in systems requiring non-causal controllers. To mitigate such challenges, constraining the imaginary part of PTO control is often employed as a sub-optimal control strategy. By setting the imaginary part of $Y_{\mathrm{pto}}(\omega)$ equal to zero, the optimal control is achieved when $Y_{\mathrm{pto}}(\omega) = G_{\mathrm{pto}}(\omega) = |Y_{\mathrm{eq}}(\omega)|$. The four different PTO control techniques have been simulated instantaneous model to find the optimal control that harvests the most energy from the same wave elevation data. The four cases are followed as:

- Case 1: Damping PTO control with fixed frequency parameters.

$$Y_{\mathrm{pto}} = |Y^*_{\mathrm{eq}}(m_a(\omega_m), b(\omega_m), k)|$$

- Case 2: Complex conjugate PTO control with fixed frequency parameters.

$$Y_{\text{pto}} = Y_{\text{eq}}^*(m_a(\omega_m), b(\omega_m), k)$$

- Case 3: Damping PTO control and instantaneous frequency model with instantaneous parameters.

$$Y_{\text{pto}} = |Y_{\text{eq}}^*(m_a(\omega(t)), b(\omega(t)), k)|$$

- Case 4: Complex conjugate PTO control and instantaneous frequency model with instantaneous parameters.

$$Y_{\text{pto}} = Y_{\text{eq}}^*(m_a(\omega(t)), b(\omega(t)), k)$$

※ Note that ω_m is the mode frequency of the power spectrum density function and m_a, b represents the equivalent radiation force coefficients based on the incoming wave frequency.

3.5 Results

The results show that complex conjugate control improves power conversion, as seen in Case 2 outperforms Case 1, and Case 4 outperforms Case 3. It was expected that control based on instantaneous estimates of the mechanical impedance (Case 4) would outperform the case in which the impedance is estimated as constant

(Case 2), however, this is not observed in the simulation. More investigation is required to explain the behavior, especially as it concerns instantaneous frequency concepts as an approximation for convolution operation.

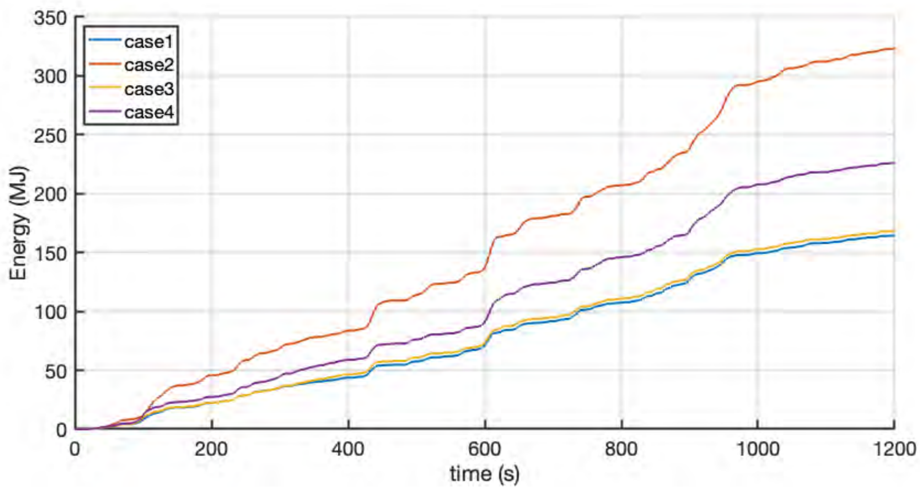

Figure 3.4: Simulation results

Cases	Total Energy	Average power
Case1	164.7 MJ	137.2 kW
Case2	323.3 MJ	269.4 kW
Case3	168.6 MJ	140.5 kW
Case4	226.1 MJ	188.5 kW

Table 3.2: Simulation Results

3.6 Conclusion

These findings demonstrate the effectiveness of the ROM model in considerably capturing the WEC's behavior compared to the WEC-Sim. The insights gained from the ROM were implemented in optimizing the control parameters through a novel conversion of mechanical to electrical dynamics into circuit representations, with a focus on synthesizing Newtonian mechanics as circuit equivalents. This approach enables the development of a circuit model that computes the forces and effects of the PTO system. The combined ROM-circuit model of a WEC can be applied to optimize the control of the PTO Force by impedance matching technique, ultimately improving the efficiency of wave energy conversion systems. The accurate and efficient nature of the ROM makes it a valuable tool for evaluating design alternatives and control strategies, which can lead to cost-effective and high-performance WEC systems.

Chapter 4: Addendum

The previous chapter introduced Power-Take-Off (PTO) control optimization using an equivalent circuit model. However, as Chapter 2 results revealed, a small but non-negligible error exists compared to WEC-Sim results. To address this discrepancy, a parallel analysis was conducted within the equivalent circuit framework, and the PTO control technique was implemented in WEC-Sim's PTO control, consistent with equivalent circuit modeling.

4.1 Real-time PTO Control Using Instantaneous frequency

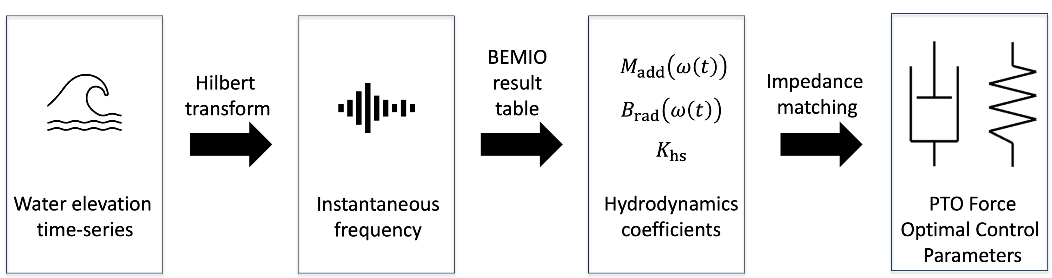

Figure 4.1: Workflow for PTO control parameters

Figure 4.1 illustrates the process of determining PTO control parameters. While the process aligns with the method presented in Chapter 3, the calculation of instantaneous frequency for WEC-Sim is performed in real-time, unlike the previous model. In Chapter 3, the model accessed the entire water elevation time series data at the simulation's initiation, enabling a single Fast Fourier Transform (FFT) calculation to establish the instantaneous frequency. While this method yields accurate frequency data, it is impractical as it necessitates complete water elevation data in advance.

To overcome this limitation, A practical real-time instantaneous frequency calculation has been integrated into WEC-Sim's Power-Take-Off (PTO) control. This entails limiting access to water elevation data to the past and current time and establishing a window size estimated by multiplying the wave peak period. The multiplication factor is set at 10. For example, assuming that the dominant period of the wave spectrum is 8 s, the past and current water elevation data for 80 s have been employed to perform the Hilbert transform at each time step as shown in Figure.4.2. Before the simulation time reaches the pre-defined window size for the Fast Fourier Transform (FFT) calculation, historical water elevation data is unavailable. During this period, the model utilizes the wave spectrum's mode frequency as a single frequency to estimate the PTO control parameters.

The pre-calculated PTO stiffness table reveals negative values within a specific wave period range of 5.063 s to 11.635 s, as illustrated in Figure 4.3. When the negative stiffness surpasses the system's hydrodynamic stiffness, it leads to device instability and potential disintegration. Consequently, a negative stiffness limit has been established to truncate the exceeded values, as shown in Figure 4.3. The truncated amount in stiffness has been compensated by adjusting the damping coefficient to match the amplitude of the equivalent admittance Y_{eq}. The peak wave periods have been selected from $T_p = 4$ s to 12 s with an increment of 1 s.

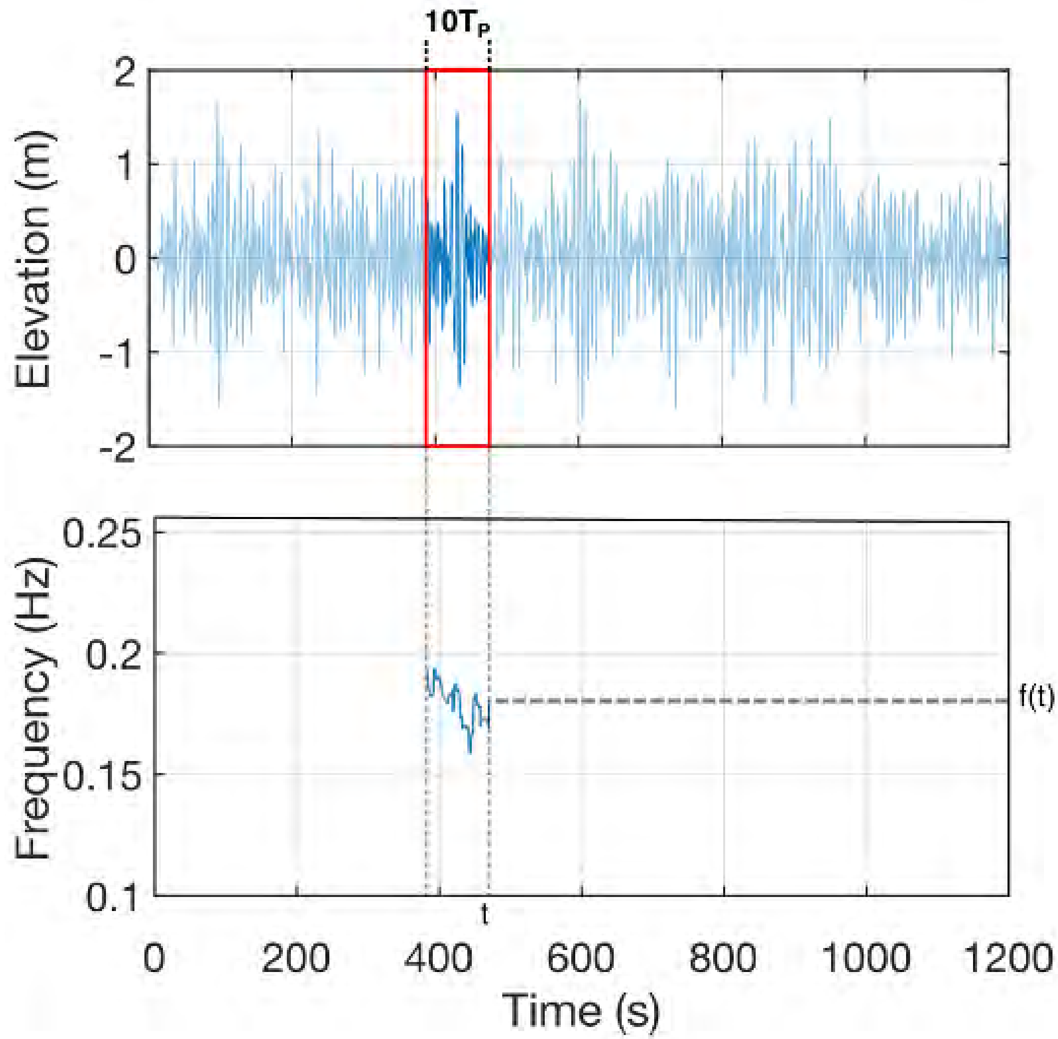

Figure 4.2: An example of real-time instantaneous frequency calculation.

For each wave peak period case, where wave data is generated from the JONSWAP spectrum with Gamma = 1 and significant wave height = 1.5 m, simulations are conducted using five different PTO force control techniques in WEC-Sim. The corresponding PTO control techniques are presented as follows:

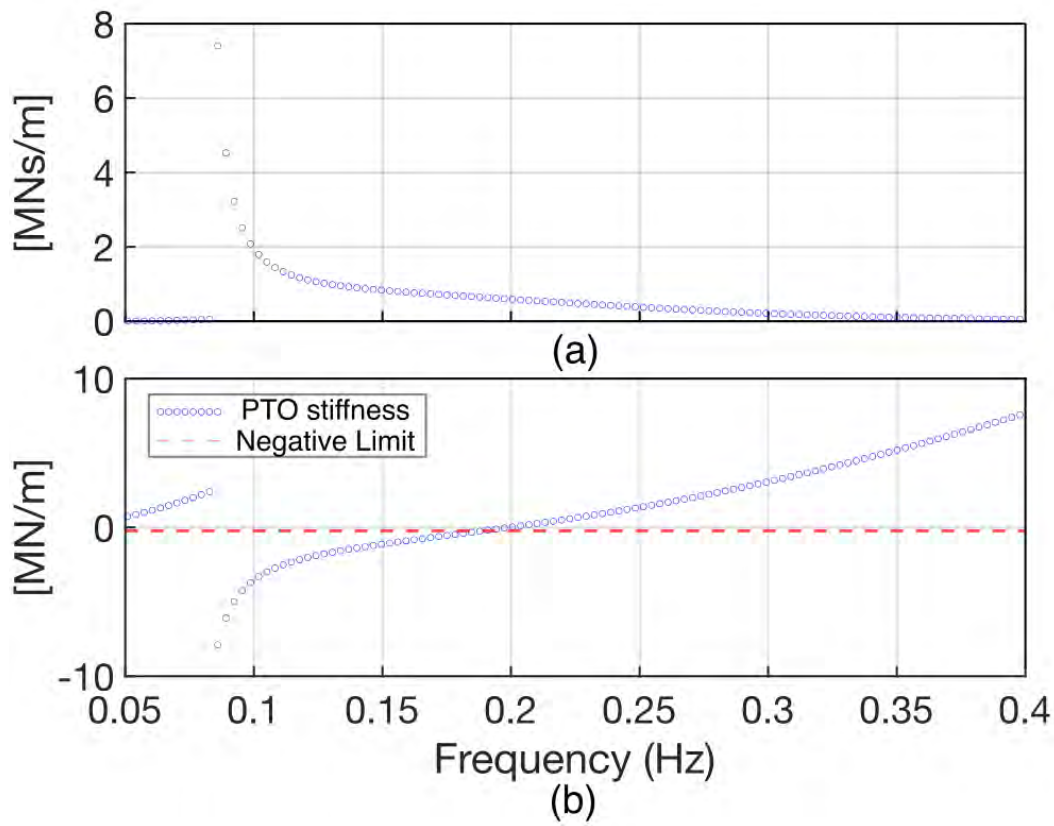

Figure 4.3: (a) damping and (b) stiffness coefficient for PTO force via eigen analysis

- Case 1: Default damping 1, 200, 000 N/m and no stiffness PTO force control.
- Case 2: Damping and no stiffness PTO force control with fixed frequency parameters.

$$Y_{\text{pto}} = |Y^*_{\text{eq}}(m_a(\omega_m), b(\omega_m), k)|$$

- Case 3: Complex conjugate damping and stiffness PTO force control with fixed frequency parameters.

$$Y_{\text{pto}} = Y_{\text{eq}}^{*}(m_a(\omega_m), b(\omega_m), k)$$

- Case 4: Damping and no stiffness PTO force control with instantaneous frequency parameters.

$$Y_{\text{pto}} = |Y_{\text{eq}}^{*}(m_a(\omega(t)), b(\omega(t)), k)|$$

- Case 5: Complex conjugate damping and stiffness PTO force control with instantaneous frequency parameters.

$$Y_{\text{pto}} = Y_{\text{eq}}^{*}(m_a(\omega(t)), b(\omega(t)), k)$$

The details of wave and simulation parameters are provided in Table 4.1 and 4.2. It is noteworthy that H_s, T_p, and γ represent significant wave height, energy peak period, and the extra peak enhancement factor gamma, where $\gamma = 1$ essentially denotes the Pierson-Moskowitz spectrum.

Parameters	**Values**
Wave spectrum	JONSWAP
H_s	1.5 m
T_p	4 s to 12 s
γ	1

Table 4.1: Wave Parameters

Parameters	**Values**
Duration	1200 s
Timestep	0.1 s
Ramptime	40 s
FFT window size	$10 * T_p$

Table 4.2: Simulation Parameters

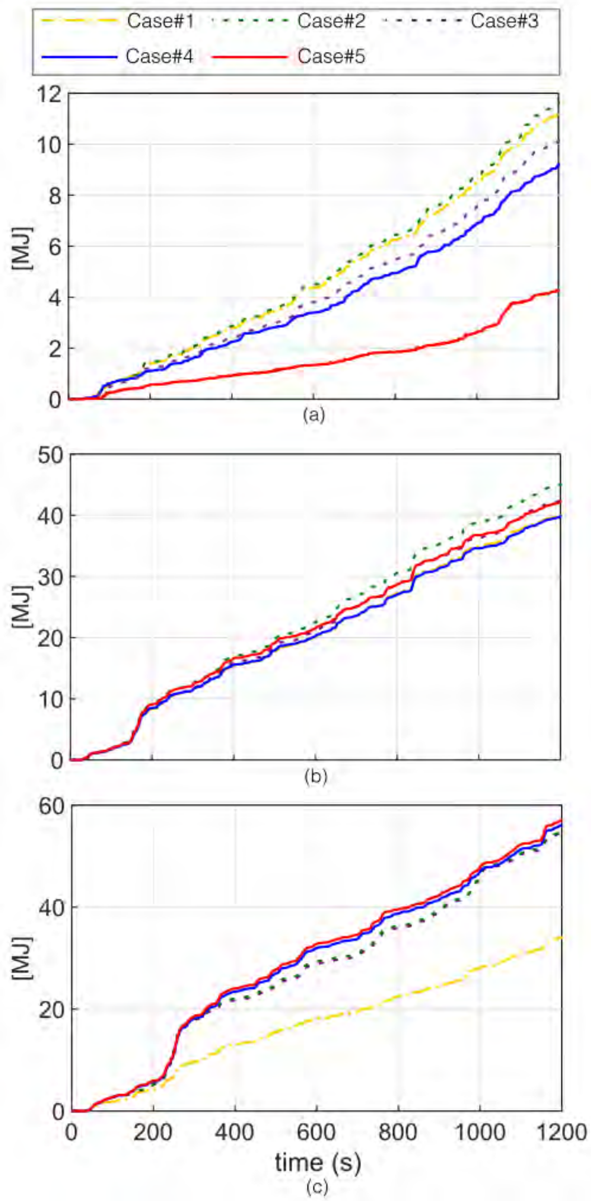

Figure 4.4: Simulation results of the accumulative energy harvested by PTO at the wave peak period of (a) $T_p = 4$ s, (b) $T_p = 8$ s, and (c) $T_p = 12$ s.

4.2 Results

The accumulated energy harvested from the PTO unit is utilized for comparison between the cases, as depicted in Figure 4.4. The default damping PTO control (Case 1) yields optimal results under faster wave conditions, specifically at 4 s and 5 s, with a peak at 9 s followed by a decline. In contrast, both real-time PTO control (cases 4 and 5) and fixed PTO parameter control (cases 2 and 3) demonstrate an increasing trend in effectiveness as the wave peak period rises, as illustrated in Figure 4.5. Case 2 demonstrates its superiority in the periods from 6 s to 9 s. Case 5 exhibits a more pronounced increase than other cases at higher peak periods, becoming the most optimal among the cases from 10 s to 12 s of the peak period.

4.3 Addendum Conclusion

A total of five different PTO control cases were simulated across nine wave peak periods. Due to limitations imposed by the structural nature of the device, optimal impedance matching control has not been achieved. Nevertheless, it is noteworthy that the real-time control using instantaneous frequency has proven effective, demonstrating remarkable results in higher wave period conditions, even though its sub-optimal parameters were applied. The anticipated lower performance of cases 2 through 5 in faster wave conditions is expected, given that eigenmode analysis predominantly indicates the heave sides and the corresponding PTO control parameters derived from that perspective. This is illustrated in Figure 2.3 in Chapter

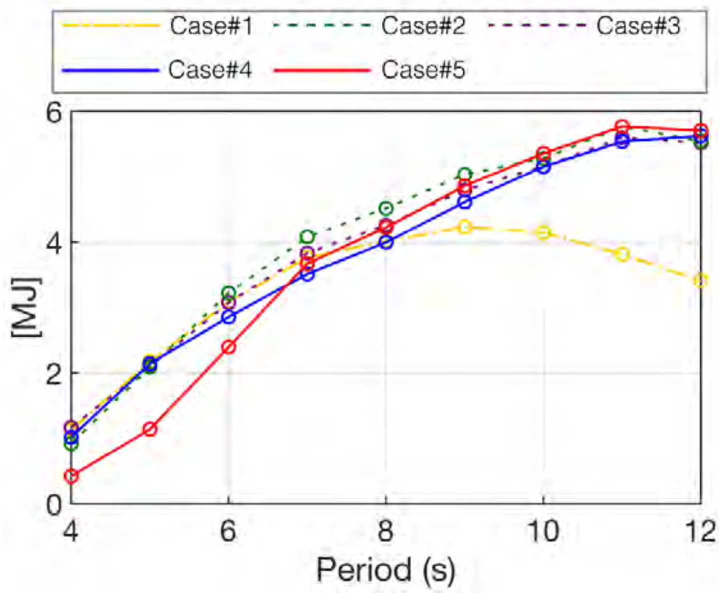

Figure 4.5: Simulation results of the accumulative energy harvested at end time versus wave peak period

2, where pitch excitation becomes the dominant factor when the wave period is lower than 5.2 s. Physically, higher-frequency waves are accompanied by shorter wavelengths. The shorter wavelength impacts the heaving excitation force on the floating body, resulting in a less pronounced heaving motion. This underscores the importance of designing WEC devices with consideration for the specific wave conditions at their deployment locations. Such considerations are vital for ensuring that the Wave Energy Converter operates in the intended motion, facilitating the implementation of optimal control to maximize energy harvest. Furthermore, the exploration of enabling more negative PTO stiffness by adjusting structural parameters, while ensuring system stability or reducing the imaginary component of the equivalent admittance, will be undertaken to implement more optimal impedance matching control in future research.

Chapter 5: General Conclusion

The application of instantaneous frequency to model wave energy conversion devices and optimize their Power Take-Off (PTO) control has been discussed in preceding chapters. Chapter 2 assesses the modeling accuracy through a combination of eigen-mode analysis and instantaneous frequency modeling in real sea conditions. Building upon the model's accuracy presented in Chapter 3, PTO force control optimization was implemented in the equivalent circuit modeling using the instantaneous frequency concept, yielding promising results. Finally, Chapter 4 demonstrates the real-time implementation of PTO control using instantaneous frequency, integrated into WEC-Sim's PTO control system.

The use of instantaneous frequency in equivalent circuit modeling provides computational benefits, thanks to its conciseness achieved through selective eigenmode analysis. This approach improves accuracy in predicting system responses in field sea conditions, including the JONSWAP and Pierson-Moskowitz waves. Additionally, by leveraging electrical circuit theory and applying the impedance matching technique to the equivalent circuit, a potential optimal control scheme has been introduced. Despite limitations imposed by mechanical constraints, it is noteworthy to confirm the functionality of the control under specific conditions, such as heave-dominant wave excitation to the devices, as discussed in Chapter 4.

In future research, the exploration of proper mechanical design to facilitate optimal impedance matching techniques, as discussed in Chapter 4, will be undertaken. Additionally, the experimental validation of these techniques could be demonstrated using the Laboratory Upgraded Point Absorber at Oregon State University.

Bibliography

[1] B. Bosma, C. Beringer, M. Leary, and B. Robertson. Design and modeling of a laboratory scale wec point absorber. In *14th European Wave and Tidal Energy Conference (EWTEC 2021)*, September 2021.

[2] T. K. A. Brekken, A. V. Jouanne, and H. Y. Han. Ocean wave energy overview and research at oregon state university. In *Power Electronics and Machines in Wind Applications*. PEMWA, 2009.

[3] L. Cohen. *Time-frequency analysis*, volume 778. Prentice Hall, New Jersey, 1995.

[4] J. Falnes and A. Kurniawan. *Ocean waves and oscillating systems: linear interactions including wave-energy extraction*, volume 8. Cambridge University Press, 2020.

[5] M. Folley and T. J. T. Whittaker. Analysis of the nearshore wave energy resource. *Renewable Energy*, 34(7):1709–1715, 2009.

[6] Y. Fu, Z. Gao, Y. Liu, A. Zhang, and X. Yin. Actuator and sensor fault classification for wind turbine systems based on fast fourier transform and uncorrelated multi-linear principal component analysis techniques. *Processes*, 8(9):1066, 2020.

[7] K. Hasselmann, T. P. Barnett, E. Bouws, H. Carlson, D. E. Cartwright, K. Enke, J. A. Ewing, A. Gienapp, D. E. Hasselmann, P. Kruseman, et al. Measurements of wind-wave growth and swell decay during the joint north sea wave project (jonswap). *Ergänzungsheft zur Deutschen Hydrographischen Zeitschrift, Reihe A*, 1973.

[8] I. Kim, N. Adami, P. Chandran, Y. Cao, B. Johnson, S. Yim, T. Brekken, and C. Beringer. Equivalent circuit modeling of a wave energy converter via eigenmode analysis. In *Proc. of Energy Conversion Congress and Exposition*, 2023.

[9] D. De Klerk, D. J. Rixen, and S. N. Voormeeren. General framework for dynamic substructuring: history, review and classification of techniques. *AIAA Journal*, 46(5):1169–1181, 2008.

[10] C. H. Lee and J. N. Newman. *Wamit user manual*, 2006. WAMIT Inc., Chestnut Hill, MA, USA, p. 42.

[11] M. K. Ochi. *Ocean Waves*. Cambridge University Press, Cambridge, UK, March 1998.

[12] S. S. Ravindran. A reduced-order approach for optimal control of fluids using proper orthogonal decomposition. *International Journal for Numerical Methods in Fluids*, 34(5):425–448, 2000.

[13] C. W. Rowley. Model reduction for fluids, using balanced proper orthogonal decomposition. *International Journal of Bifurcation and Chaos*, 15(03):997–1013, 2005.

[14] Y.-H. Y. A. K. N. T. D. F. J. L. J. G. S. H. Kelley Ruehl and David Ogden. Wec-sim v5.0.1. `https://zenodo.org/badge/latestdoi/20451353`, September 2022.

[15] Z. Yu and J. Falnes. State-space modeling of a vertical cylinder in heave. *Applied Ocean Research*, 17(5):265–275, 1995.